5. P. A. Reasenberg and R. W. Simpson, *Science* **255**, 1687 (1992).
6. J. R. Rice, in *Fault Mechanics and Transport Properties of Rock*, B. Evans and T.-F. Wong, Eds. (Academic Press, London, 1992), pp. 475.
7. R. S. Stein and M. Lisowski, *J. Geophys. Res.* **88**, 6477 (1983). The moment used for the Homestead Valley earthquake includes postseismic slip, consistent with measured deformation from 1979 to 1981.
8. D. H. Oppenheimer, P. A. Reasenberg, R. W. Simpson, *J. Geophys. Res.* **93**, 9007 (1988).
9. K. W. Hudnut, L. Seeber, J. Pacheco, *Geophys. Res. Lett.* **16**, 199 (1989); S. Larsen, R. Reilinger, H. Neugebauer, W. Strange, *J. Geophys. Res.* **97**, 4885 (1992).
10. R. W. Simpson and P. A. Reasenberg, *U.S. Geol. Surv. Prof. Pap.*, in press.
11. M. Lisowski, J. C. Savage, and W. H. Prescott [*J. Geophys. Res.* **96**, 8369 (1991)] found a principal contractive strain rate of N7 ± 1°E from trilateration surveys conducted since 1979 in the Joshua geodetic network, which includes most of the Landers rupture. J. Sauber, W. Thatcher, and S. C. Solomon [*J. Geophys. Res.* **91**, 12683 (1986)] found that the most compressive principal strain direction measured from 1934 to 1982 across the north half of the Landers rupture was N4 ± 5°E from triangulation surveys.
12. L. M. Jones, *J. Geophys. Res.* **93**, 8869 (1988). The mean of the principal stress directions for the two segments that abut the Landers site, Banning and Indio, is N6 ± 2°E. P. L. Williams, L. R. Sykes, C. Nicholson, and L. Seeber [*Tectonics* **9**, 185 (1990)] found that an average principal stress direction for the adjacent 50-km stretch of the San Andreas fault (San Gregorio Pass and Eastern Transverse Range-I regions) was N8 ± 5°E.
13. C. DeMets, R. G. Gordon, D. F. Argus, S. Stein, *Geophys. J. Int.* **101**, 425 (1990). The Pacific–North American plate motion vector for central California is N36 ± 2°W, which yields a principal compression oriented N9 ± 2°W.
14. M. D. Zoback and J. H. Healy, *J. Geophys. Res.* **97**, 5039 (1992). The Cajon Pass well yields an N57 ± 19°E principal stress direction. If permanent, this stress could not drive local right-lateral slip on the San Andreas fault, and has been interpreted to suggest that the San Andreas is a weak (low μ) fault embedded in a strong (high μ) crust [see M. D. Zoback and A. H. Lachenbruch, *ibid.*, p. 4991]. The stress measured in the well may be influenced by local faults (G. Shamir and M. D. Zoback, *ibid.*, p. 5059) and thus not represent a regional value.
15. All earthquakes in this study except North Palm Springs occurred on near vertical faults with dominant strike slip. We simulated the 30% dip-slip component and 59° dip of the North Palm Springs rupture by including a fault-closing (for example, dike deflation) displacement equal to cos(rake) × cos(dip). This approximation gives accurate stresses at distances greater than one fault length from the source.
16. The mean static shear stress drop calculated from the parameters in Table 1 following H. Kanamori and D. L. Anderson [*Bull. Seismol. Soc. Am.* **65**, 1073 (1975)].
17. C. E. Johnson and D. P. Hill, *U.S. Geol. Surv. Prof. Pap. 1254*, 15 (1982); S. H. Hartzell and T. H. Heaton, *Bull. Seismol. Soc. Am.* **73**, 1553 (1983); T. C. Hanks and C. R. Allen, *ibid.* **79**, 231 (1989); K. Hudnut *et al.*, *ibid.*, p. 282 (1989).
18. Landers aftershocks could be absent in the Coachella Valley because the total stress there is lower or because the strength is higher. We examined the effect of a low modulus Mojave tectonic block embedded in a stiffer crust, consistent with the P_g velocity contours of T. M. Hearn and R. W. Clayton [*Bull. Seismol. Soc. Am.* **76**, 495 (1986)]. The average velocity contrast between the Mojave region (100 by 300 km) with P_g velocity <6.2 km/s and the surrounding medium is 0.45 km/s. We gave the Mojave block a Young's modulus, E, of 6.2×10^{11} dyne-cm^{-2} bars. In this plane stress calculation, the Coulomb failure stress increase was halved in the Coachella Valley, but is nearly unchanged elsewhere. Thus it is possible that we overestimated the stress change for the Coachella Valley in Figs. 3 and 4.
19. Working Group on California Earthquake Probabilities, *U.S. Geol. Surv. Open-File Rep. 88-398* (1988).
20. Site of the 1948 **M** = 6.0 Desert Hot Spring earthquake; see L. R. Sykes and L. Seeber, *Geology* **13**, 835 (1985).
21. Monitoring with Global Positioning System networks has not detected postseismic slip greater than several centimeters across the San Andreas fault at Cajon Pass and in the Coachella Valley (M. Lisowski, personal communication).
22. G. C. Jacoby, Jr., P. R. Shepard, K. E. Sieh, *Science* **241**, 196 (1988); K. Sieh, M. Stuiver, D. Brillinger, *J. Geophys. Res.* **94**, 603 (1989).
23. R. J. Weldon II and K. E. Sieh, *Geol. Soc. Am. Bull.* **96**, 793 (1985); R. J. Weldon II, thesis, California Institute of Technology (1986).
24. A. G. Lindh, in *Earthquake Prediction: Present Status*, S. K. Guha and A. M. Patwardhan, Eds. (University of Poona, Pune, India, 1988), p. 189. Repeat times for the Coachella Valley segment are based on K. E. Sieh, *Eos* **67**, 1200 (1986).
25. R. L. Hill and D. J. Beeby, *Geol. Soc. Am. Bull.* **88**, 1378 (1977); A. Lindh, G. Fuis, C. Mantis, *Science* **201**, 56 (1978).
26. N. E. King, D. C. Agnew, F. Wyatt, *Bull. Seismol. Soc. Am.* **78**, 1693 (1988).
27. J. C. Savage, M. Lisowski, W. H. Prescott, *Eos* **73** (Fall Suppl.), 364 (1992).
28. L. M. Jones, K. Hutton, D. A. Given, C. R. Allen, *Bull. Seismol. Soc. Am.* **76**, 1830 (1986).
29. J. Pacheco and J. Nábelek, *ibid.* **78**, 1907 (1988); S. Hartzell, *J. Geophys. Res.* **94**, 7515 (1989).
30. C. J. Ammon, A. A. Velasco, T. Lay, in preparation.
31. Preliminary broad band measurements of the Landers and Big Bear seismic moments are from H. K. Thio and H. Kanamori and from G. Ekström (personal communication).
32. Fault slip function from preliminary fault mapping by D. Ponti, M. Rymer, and K. Lajoie and from K. Sieh, K. Hudnut, C. Rubin, and T. Rockwell (personal communication).
33. We thank A. Nur, R. Weldon II, W. Thatcher, L. Jones, and J. Savage for thoughtful reviews and R. Simpson and R. Harris for stimulating discussion. We are grateful for financial support from the Southern California Earthquake Center.

25 August 1992; accepted 22 October 1992

Accumulation of Suspended Barite at Mesopelagic Depths and Export Production in the Southern Ocean

Frank Dehairs, Willy Baeyens, Leo Goeyens

The relation between the accumulation of barite ($BaSO_4$) microcrystals in suspended matter from the mesopelagic depth region (100 to 600 meters) and the type of production in the euphotic layer (new versus recycled) was studied for different Southern Ocean environments. Considerable subsurface barite accumulated in waters characterized by maintained new production and limited grazing pressure during the growth season. On the other hand, little if any barite accumulated in areas where relatively large amounts of photosynthetically fixed carbon were transferred to the microheterotrophic community and where recycled production became predominant.

In the pelagic oceanic environment, microcrystalline barite (~1 μm) precipitates during the process of organic matter degradation (*1*, *2*). This barite accounts for between 50 and 100% of the total Ba in oceanic suspended matter (*1*–*3*). Although the mechanism of barite formation is unknown, it has been suggested that during degradation of planktonic proteinaceous material sufficient sulfate is produced that barite reaches saturation and barite crystals form (*2*). This seems to be precipitation confined to microenvironments composed of aggregates of biogenic detritus (*1*–*4*). Supersaturation conditions for barite inside microenvironments can account for the presence of barite in seawater that is undersaturated (*5*). The settling of barite crystals associated with this biogenic detritus to the deep sea and its sediments can explain the observed relation between barite accumulation in the sediments and productivity in overlying surface waters (*6*). Recently, observations of particulate Ba fluxes, as sampled by sediment trap in the intermediate and deep water column, highlight the strong relation between barite and productivity and stress the potential for sedimentary barite fluxes to provide quantitative information on the paleoproductivity of the oceans (*7*). However, part of the detrital aggregates formed in surface waters decompose at mesopelagic depths (*2*, *3*). During this process, the carried barite is released as discrete crystals. This release leads to a maximum in the amounts of particulate Ba at depths of 100 to 600 m. Such a maximum is characteristic of large sections of the world ocean, including the Southern Ocean (*1*, *2*, *8*, *9*). Here, we focus on the relation between barite accumulation in mesopelagic waters and the type of production in the euphotic layer of the ocean and compare different Southern Ocean environments.

Analytical Chemistry Department, Vrije Universiteit Brussel, Pleinlaan 2, B-1050 Brussels, Belgium.

We used data obtained during four cruises in the Southern Ocean: INDIGO 3, from January to February 1987, in the Indian sector of the Southern Ocean; EPOS LEG 2, from November to December 1988, in the Scotia-Weddell Confluence area; ANTARKTIS IX/2, from October to December 1990, in the Weddell gyre; and AURORA AUSTRALIS Voyage 6, from January to March 1991, in the Indian sector and Prydz Bay. These are different environments, characterized by different ice cover zones (*10*) including: (i) the open ocean zone (OOZ), which can be covered by ice in winter but is unaffected by ice melting during summer, (ii) the marginal ice zone (MIZ) adjacent to the retreating pack ice and characterized by a shallow mixed layer, (iii) the closed pack ice zone (CPIZ), where perennial ice covers over 60% of the sea surface, and (iv) the coastal and continental shelf zone (CCSZ), which extends over the shallow shelf and is largely influenced by ice-shelf melting. These areas are each characterized by different values of seasonal nitrate depletion, ammonium availability, *f* ratios (the ratio of nitrate uptake over the summed N uptake), and subsurface total particulate Ba content (Table 1). Here, summed N uptake represents nitrate plus ammonium uptake; we did not examine uptake of urea or other recycled N compounds. Because total Ba is carried mainly by barite, we refer to total particulate Ba as Ba-barite. Details of sampling and analysis procedures are as described (*9, 11–15*); data on dissolved O_2 and nitrate taken during the Prydz Bay expedition are listed elsewhere (*16*).

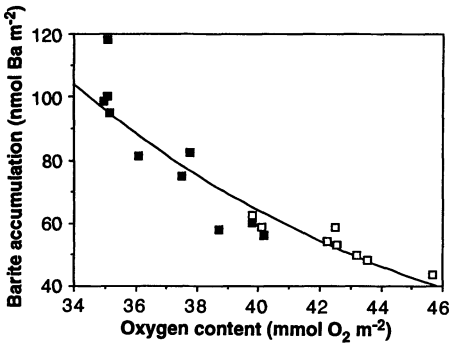

Fig. 1. Subsurface Ba-barite stocks versus dissolved O_2 stocks in the OOZ (Indian Ocean sector). These stocks represent concentrations integrated over a depth interval of 200 m centered on the Ba-barite maximum and the O_2 minimum. Closed squares, data obtained during the 1987 INDIGO 3 expedition (*9*); open squares, data obtained for the off-shelf region during the 1991 Prydz Bay expedition.

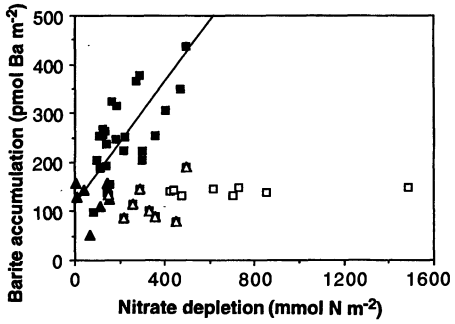

Fig. 2. Particulate Ba-barite concentrations in the mesopelagic depth region versus nitrate depletion. Data for Ba represent depth-weighted average concentrations. Closed squares, data for the OOZ; open squares, data for the CCSZ; closed triangles, data for the CPIZ; open triangles, data for the MIZ. The linear regression is based on the OOZ and CPIZ data.

The capacity of phytoplankton to support production at higher trophic levels and to shunt organic matter out of the pelagic food web is generally assessed in terms of new and regenerated production. New production refers to phytoplanktonic productivity fueled with allochthonous N sources, mainly nitrate, whereas regenerated production is derived from nutrients such as ammonium and urea, which are regenerated in situ (*17*). If the system is to maintain itself at steady state, the nitrate input through turbulent diffusion and upwelling from the deep has to be balanced by an output, associated with either organisms and biogenic particles or dissolved organic matter, of N from the euphotic layer. New production provides a measure of the upper limit of production that can be exported (*18*). The importance of new and regenerated production is judged by means of isotope (^{15}N) incorporation studies (*19*). Nitrate uptake reflects new production, whereas ammonium uptake reflects regenerated production. Their relative contribution to primary production is estimated by the *f* ratios, as defined by Eppley and Peterson (*18*).

For the open ocean area of the antarctic circumpolar current (ACC; Indian Ocean sector), the depth intervals of the maximum Ba-barite concentration (Ba-barite maximum) and the minimum O_2 concentration (O_2 minimum) appear to coincide (*9, 11*). Furthermore, a tight inverse relation between dissolved O_2 content in the O_2 minimum layer and Ba-barite content in the Ba-barite maximum layer was observed (*9, 11*). Our recent data obtained for the off-shelf area of Prydz Bay confirm this relation (Fig. 1). These observations indicate that, for the mesopelagic area, the accumulation of discrete barite crystals is linked to the amount of organic matter oxidized and thus mesopelagic barite has the potential to be used as a tracer for export production. Furthermore, for the ACC including the Scotia Sea, subsurface Ba-barite accumulation also increases as nitrate is depleted (*11*). These different observations, pertaining to the OOZ system, suggest that there is a causal relation between new production and subsurface barite accumulation.

However, the situation becomes more complex in the MIZ and CCSZ. For these environments, the data (Table 1) show that the amounts of nitrate removed by phytoplankton largely exceeded those observed in the OOZ and CPIZ. This difference reflects higher productivities in the MIZ and CCSZ. Previous studies (*20, 21*) confirm the presence of increased biomasses and productivities in the immediate vicinity of ice edges, in contrast to the generally low productivities observed in other environments of the Southern Ocean (*22*). These large nitrate depletions in the MIZ and CCSZ do not coincide with any enhancement of subsurface Ba-barite (Fig. 2 and Table 1) as expected from the results for the OOZ. They do, however, coincide with significant ammonium availabilities. Proportionally to nitrate depletion, these ammonium availabilities are even larger in the MIZ and CCSZ as compared to the CPIZ and OOZ (Table 1). Furthermore, in the MIZ and the CCSZ the absence of a significant time lag between the appearance of nitrate depletion and the appearance of ammonium indicates that there was a strikingly

Table 1. Nitrogen and particulate Ba signature in different Southern Ocean subregions. Nitrate depletion is the depth-integrated difference between in situ nitrate concentrations and the concentration in the temperature minimum layer, which reflects the winter condition (*33*). It represents a conservative estimate of the nitrate removed by phytoplankton during the ongoing growth season. Ammonium availability is the molar fraction of ammonium, in percent, in the total inorganic N pool. The relative contribution of new production to total primary production is estimated by the *f* ratio, the ratio of nitrate uptake to total N uptake, as defined by Eppley and Peterson (*18*). Mesopelagic barite accumulation is defined as the depth-weighted average Ba concentration for the depth interval where the Ba-barite maximum is located (150 to 600 m). Values represent averages ± 1 SD; for *f* ratios, maximum (max.) and minimum (min.) values are given.

Subregion	Nitrate depletion (mmol N m^{-2})	Ammonium availability (%)	*f* Ratio (max. to min.)	Subsurface Ba-barite (pmol Ba liter^{-1})
OOZ	176 ± 71	0.9 ± 0.7	0.51 to 0.45	275 ± 73
MIZ	344 ± 177	3.2 ± 1.7	0.77 to 0.30	118 ± 37
CCSZ	570 ± 281	4.6 ± 3.7	0.66 to 0.21	142 ± 6
CPIZ	47 ± 49	0.7 ± 0.4	0.82 to 0.50	281 ± 82

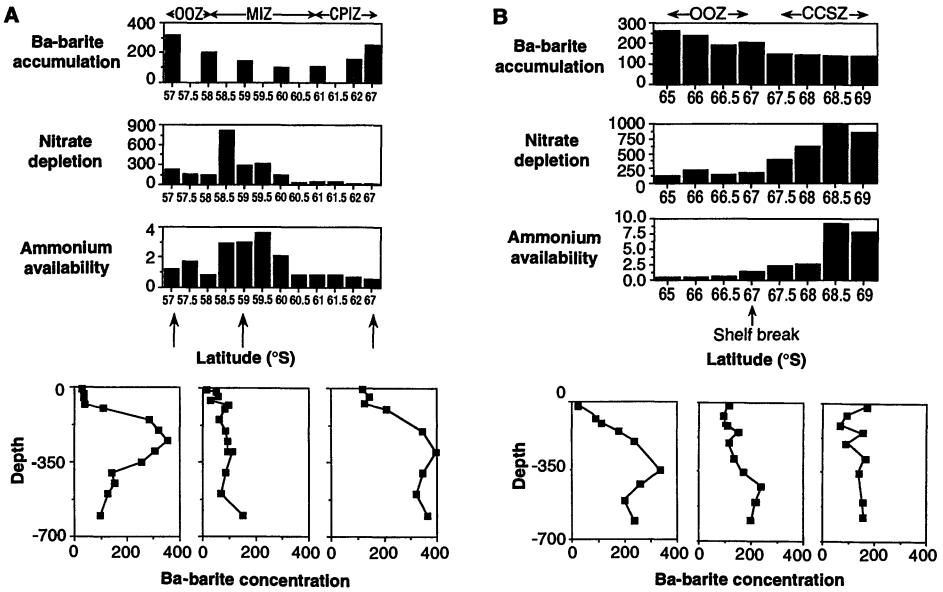

Fig. 3. Latitudinal distribution of particulate Ba-barite (picomoles of Ba per liter) in the mesopelagic depth region; nitrate depletion (millimoles of N per square meter); and ammonium availability (percent) in (**A**) the Scotia-Weddell Confluence area and (**B**) the off-shelf and on-shelf area of Prydz Bay. Data for Ba and ammonium availability represent depth-weighted average values. The arrows indicate the geographical position of the vertical particulate Ba-barite profiles (picomoles of Ba per liter); depth is in meters.

rapid response of the heterotrophic community to the onset of the bloom. This pattern is suggestive of the dominance of micrograzers (*15, 23*). In the MIZ of the Scotia-Weddell Confluence, nearly 70% of the net primary production was assimilated in the microbial food loop of bacterioplankton, heteronanoflagellates, and protozoa (*23*). Copepods and other macrozooplankton generally contribute, to a minor extent, to ammonium production (*24*). Increases in ammonium concentration can enhance the ammonium uptake rate and reduce the nitrate uptake rate (*25*). We observed drastic decreases in the *f* ratio concurrent with increasing ammonium availability (*14*), whereas high *f* ratios prevailed in areas where ammonium was less abundant (Table 1).

Our observations indicate that the export of organic particulates, reflected by the mesopelagic Ba-barite accumulation, is significant in the OOZ and CPIZ, which are characterized by moderate nitrate depletions and a small ratio of ammonium availability to nitrate depletion. On the other hand, export appears not to be significant in the MIZ and CCSZ systems, which have much larger nitrate depletions and large ratios of ammonium availability to nitrate depletion (Table 1). These differences in production and export between the studied environments are well illustrated by two north-to-south transects: the first one in the Scotia-Weddell Confluence area and the Weddell Sea (57° to 68°S) and the second one in the Prydz Bay slope and shelf region (Indian sector, 65° to 69°S). For the Scotia-Weddell Confluence (Fig. 3A), the northernmost stations, located in an OOZ system (Scotia Sea), showed the largest subsurface Ba-barite accumulations (300 pmol of Ba liter^{-1}) and the development of a clear subsurface maximum. The MIZ showed small Ba-barite accumulations (down to 100 pmol of Ba liter^{-1}) and no development of a distinct subsurface Ba-barite maximum, whereas nitrate depletion (up to 800 mmol of N m^{-2}) and ammonium availabilities (up to 3.6%) were maximal. In the area of extended ice cover (CPIZ), nitrate depletions and ammonium availabilities decreased drastically (nitrate depletion was down to 35 mmol of N m^{-2}; ammonium availability was down to 0.5%), whereas mesopelagic Ba-barite accumulations increased again and reached values similar to those in the OOZ and showed a distinct subsurface Ba-barite maximum. This peculiar situation in the CPIZ is explained below. For the Prydz Bay area (Fig. 3B), the off-shelf region (OOZ) showed a large subsurface Ba-barite accumulation (270 pmol of Ba liter^{-1}) and moderate nitrate depletions and ammonium availabilities (125 mmol of N m^{-2} and 0.5%, respectively). Vertical profiles of particulate Ba in the OOZ clearly show that a subsurface maximum had developed. Within the shelf region (CCSZ), the Ba-barite contents decreased (concentrations down to 110 pmol of Ba liter^{-1}), whereas nitrate depletions and ammonium availabilities abruptly increased to reach high values (nitrate depletion up to 1000 mmol of N m^{-2}; ammonium availability up to 9%) in the vicinity of the Amery Ice Shelf. These examples illustrate that the areas with the highest productivities, as reflected by the magnitude of nitrate depletion, are not necessarily those characterized by the largest export of production.

Different studies in the Weddell Sea and the Ross Sea (*26, 27*) as well as along the Antarctic Peninsula and adjacent islands (*28, 29*) and in Prydz Bay near the Amery Ice Shelf indicate that intensive phytoplankton blooms occur mainly in well-sheltered and stabilized waters near pack ice or ice-shelf edges. In such areas, the fast development of the phytoplankton bloom, reflected by large nitrate removal during a 2- to 3-week period, initiates the development of an important micrograzer community keeping close pace with the autotrophs (*23*). This considerable grazing pressure is reflected by enhanced ammonium buildup, which in turn triggers the installation of a system based on regenerated production. The resulting considerable organic matter flow into the microbial food loop does not leave room for important export. Hence, at mesopelagic depths no significant buildup of barite stocks occurs in these areas.

On the contrary, in the less productive CPIZ and OOZ, characterized by moderate to low nitrate depletions and ammonium availabilities, new production remains in excess of, or close to, 50% of total production during the growth season (Table 1). The development of blooms worthy of that term is inhibited by a deepening of the upper mixed layer because of wind stress in the OOZ (*30*) and by poor light availability in the CPIZ (*31*). As a consequence, development of the grazer community most likely is suppressed, and grazing pressure is relatively less important. For the OOZ and CPIZ, this grazing pressure and resulting ammonium release are not sufficient for recycled production to dominate primary production. Much of the moderate primary production remains available for export. Even in absolute terms, export in the OOZ system is likely to exceed export in the MIZ and CCSZ systems, although the latter are characterized by a larger total production. For CPIZ systems, the considerable Ba-barite accumulations suggest that export will be of magnitude similar to that in the OOZ. This possibility is difficult to reconcile with the generally low primary production of the pelagic phytoplankton in this environment (*31*). In the CPIZ, however, account has to be taken of the production by ice algae. Indeed, ice algae reveal a strong propensity to form aggregates when released in the water column, and this can contribute significantly to the vertical flux of matter (*32*), thus providing for signifi-

cant export in the CPIZ despite low productivities in the water column.

REFERENCES AND NOTES

1. F. Dehairs, R. Chesselet, J. Jedwab, *Earth Planet. Sci. Lett.* **49**, 528 (1980).
2. J. K. B. Bishop, *Nature* **332**, 341 (1988).
3. N. Stroobants, F. Dehairs, L. Goeyens, N. Vanderheyden, R. Van Grieken, *Mar. Chem.* **35**, 411 (1991).
4. T. J. Chow and E. D. Goldberg, *Geochim. Cosmochim. Acta* **20**, 192 (1960).
5. T. M. Church and K. Wolgemuth, *Earth Planet. Sci. Lett.* **15**, 35 (1972).
6. K. K. Turekian and E. H. Tausch, *Nature* **201**, 696 (1964).
7. J. Dymond, E. Suess, M. Lyle, *Paleoceanography* **7**, 163 (1992).
8. F. Dehairs, C. E. Lambert, R. Chesselet, N. Risler, *Biogeochemistry* **4**, 119 (1987).
9. F. Dehairs *et al.*, *Global Biogeochem. Cycles* **4**, 85 (1990).
10. P. Tréguer and G. Jacques, *Polar Biol.* **12**, 149 (1992).
11. F. Dehairs, N. Stroobants, L. Goeyens, *Mar. Chem.* **35**, 399 (1991).
12. F. Dehairs, L. Goeyens, N. Stroobants, S. Mathot, *Polar Biol.* **12**, 25 (1992).
13. A. Poisson, B. Schauer, C. Brunet, *Les Rapports des Campagnes à la Mer, MD 53/INDIGO 3 à bord du Marion Dufresne* (Publications de la Mission de Recherche des Terres Australes et Antarctiques Françaises, Paris, 1990).
14. L. Goeyens *et al.*, *Mar. Ecol. Prog. Ser.* **77**, 7 (1991).
15. L. Goeyens *et al.*, *ibid.* **78**, 241 (1991).
16. B. Tilbrook, personal communication.
17. R. C. Dugdale and J. J. Goering, *Limnol. Oceanogr.* **12**, 196 (1967).
18. R. W. Eppley and B. J. Peterson, *Nature* **282**, 677 (1979).
19. W. G. Harrison, in *Nitrogen in the Marine Environment*, E. J. Carpenter and D. G. Capone, Eds. (Academic Press, New York, 1983), pp. 763–807.
20. W. O. Smith, Jr., and D. M. Nelson, *Bioscience* **36**, 251 (1986).
21. C. W. Sullivan, C. R. McClain, J. C. Comiso, W. O. Smith, Jr., *J. Geophys. Res.* **93**, 12487 (1988).
22. O. Holm-Hansen, S. Z. El-Sayed, G. A. Franceschini, R. L. Cuhel, in *Adaptation Within Antarctic Ecosystems*, G. A. Llano, Ed. (Gulf Publishing, Houston, 1977), pp. 11–50.
23. C. Lancelot, G. Billen, C. Veth, S. Becquevort, S. Mathot, *Mar. Chem.* **35**, 305 (1991).
24. D. C. Biggs, *Polar Biol.* **1**, 55 (1982).
25. W. O. Smith, Jr., and G. W. Harrison, *Deep-Sea Res.* **38**, 1463 (1991).
26. W. O. Smith, Jr., and D. M. Nelson, *Limnol. Oceanogr.* **35**, 809 (1990).
27. D. M. Nelson and W. O. Smith, Jr., *Deep-Sea Res.* **33**, 1389 (1986).
28. B. G. Mitchell and O. Holm-Hansen, *ibid.* **38**, 981 (1991).
29. N. J. P. Owens, J. Priddle, M. J. Whitehouse, *Mar. Chem.* **35**, 287 (1991).
30. E. Sakshaug, D. Slagstad, O. Holm-Hansen, *ibid.*, p. 259.
31. S. Mathot, J. M. Dandois, C. Lancelot, *Polar Biol.* **12**, 321 (1992).
32. U. Riebesell, I. Schloss, V. Smetacek, *ibid.* **11**, 239 (1991).
33. J. C. Jennings, Jr., L. I. Gordon, D. M. Nelson, *Nature* **309**, 51 (1984).

34. F.D. is a research associate at the National Fund for Scientific Research, Belgium. This research is part of the Belgian Scientific Research Program on Antarctic Research. It was made possible thanks to the cooperation of Terres Australes et Antarctiques Françaises, the Alfred Wegener Institute for Polar and Marine Research, Australian Antarctic Division, and the European Science Foundation. We thank the two anonymous reviewers for their comments and criticisms.

10 June 1992; accepted 17 September 1992

X-ray Detection of the Period-Four Cycling of the Manganese Cluster in Photosynthetic Water Oxidizing Enzyme

Taka-aki Ono,* Takumi Noguchi, Yorinao Inoue, Masami Kusunoki, Tadashi Matsushita, Hiroyuki Oyanagi

X-ray absorption near-edge structure spectra of the manganese (Mn) cluster in physiologically native intermediate states of photosynthetic water oxidation induced by short laser flash were measured with a compact heat-insulated chamber equipped with an x-ray detector near the sample surface. The half-height energy of the Mn K-edge showed a period-four oscillation dependent on cycling of the Joliot-Kok's oxygen clock. The flash number–dependent shift in the Mn K-edge suggests that the Mn cluster is oxidized by one electron upon the S_0-to-S_1, S_1-to-S_2, and S_2-to-S_3 transitions and then reduced upon the S_3-to-S_0 transition that releases molecular oxygen.

Atmospheric oxygen is a result of water cleavage by oxygenic photosynthesis in plants. The fundamental view of the mechanism of photosynthetic water oxidation was introduced by Joliot *et al.*, who first found the period-four oscillation of oxygen evolution under flashing light (*1*). The oscillation suggested that the water-oxidizing machinery becomes sequentially oxidized through five different intermediate states, denoted as S_i (i = 0 to 4), to evolve molecular oxygen through the cumulative use of the energy of four photons (*2*). Much circumstantial evidence has suggested that the chemical entity of the machinery is a tetranuclear Mn cluster (*3*, *4*). However, this generally accepted concept still lacks conclusive evidence because of the difficulty in monitoring the chemical or electronic state of Mn at each S-state by a direct detection method. We report an entire set of x-ray absorption near-edge structure (XANES) spectra of the Mn cluster at respective S-states, generated under physiological conditions by a series of laser flashes, that reveals a characteristic period-four oscillation of the Mn K-edge energy. These spectra are indicative of a period-four change in the oxidation state or electronic environment, or both, of the Mn cluster. The results demonstrate that every reaction step of the S-state turnovers involves a direct reaction of Mn.

X-ray absorption spectroscopy has been successfully applied to detect oxidation of Mn upon S_2 formation (*5*–*9*). In these experiments, the S_2-state was accumulated in a dense photosystem II (PSII) sample by continuous light illumination at a cryogenic temperature. In flashing light experiments, however, the sample concentration must be low enough to ensure light saturation by a short flash. In order to measure a high-quality XANES spectra of dilute PSII samples, we designed a compact heat-insulation chamber equipped with an x-ray detector that was 1.5 cm from the sample surface, which enabled us to collect the fluorescent x-ray from Mn at high efficiency. The processed XANES spectra of PSII membranes after zero to five flashes are presented in Fig. 1A along with the original data points. The K-edge of the spectrum changed with the flash number, as is shown more clearly by Fig. 1B, in which all five spectra are displayed on the same expanded energy scale after correction of background baseline (*8*). The half-height energy of the Mn K-edge was estimated to be 6551.7 ± 0.2 eV for dark-adapted PSII (S_1-state) but was upshifted by 0.7 eV after one flash (S_2-state). Both of these two K-edge energy values and the K-edge upshift upon the S_1-to-S_2 transition are consistent with those reported previously (*6*, *8*, *9*). The relatively small extent of the upshift compared with the reported value (~1 eV) is due to both dissipation of the S_2-state by reduction by tyrosin D and incompleteness of the S_1-to-S_2 transition by misses (see legend to Fig. 2). The upshift of Mn K-edge energy has been interpreted to mean that Mn(III) is oxidized to Mn(IV) as the S_2-state is accumulated by continuous illumination at a cryogenic temperature (*5*–*9*). Thus our results indicate that oxidation of Mn occurs upon the formation of physiologically native S_2-state by a single flash given at room temperature. The half-height energies of our spectra were determined to be 6552.4 ± 0.2, 6553.4 ± 0.2, 6551.5 ± 0.2, 6551.7 ± 0.2, and 6552.0 ± 0.2 eV after 1, 2, 3, 4, and 5 flashes, respectively.

T. Ono, T. Noguchi, Y. Inoue, Solar Energy Research Group, Institute of Physical and Chemical Research (RIKEN), Wako, Saitama 351-01, Japan.
M. Kusunoki, School of Science and Technology, Meiji University, Kawasaki, Kanagawa 214, Japan.
T. Matsushita, Photon Factory, National Laboratory for High Energy Physics, Tsukuba, Ibaraki 305, Japan.
H. Oyanagi, Electrotechnical Laboratory, Tsukuba, Ibaraki 305, Japan.

*To whom correspondence should be addressed.